Phenomenological analysis of dispersion corrections for neutron and proton scattering from ^{208}Pb

R. W. Finlay, J. Wierzbicki, and R. K. Das
Ohio University, Athens, Ohio 45701

F. S. Dietrich
Lawrence Livermore National Laboratory, Livermore, California 94550
(Received 23 May 1988; revised manuscript received 17 November 1988)

Elastic scattering of protons and neutrons from ^{208}Pb in the energy range up to 61.4 MeV is analyzed in order to establish a consistent phenomenology with which to examine the recent results of dispersion theory. The present analysis avoids conventional assumptions about the energy dependences of potential depths or geometrical parameters and attempts to include estimates of the uncertainty in our knowledge of the derived potential parameters. Recently reported evidence for energy-dependent geometrical parameters in the $n+^{208}$Pb potential is supported by the present analysis, but no comparable effect is observed for phenomenological proton potentials in the range of available data ($E_p > 9$ MeV). The present analysis shows that, unlike the situation for heavy-ion scattering, the Coulomb potential does not cut off the imaginary potential for $p+^{208}$Pb. Consequently, no rapid excursions in the parameters of the $p+^{208}$Pb potential are expected to occur until the incident energy is well below the Coulomb barrier where the nuclear potential is essentially unobservable.

I. INTRODUCTION

After more than five decades of observation of nucleon-nucleus scattering, it should be possible to construct a satisfactory representation of this basic process, but it should not be surprising to learn that the reaction mechanisms are more complicated than our simplest potential models. For example, recent observation[1-3] of a rapid energy dependence of the geometrical parameters of the $n+^{208}$Pb optical potential has been interpreted as evidence for the dispersion correction to the optical potential. A dispersion correction was discussed by Feshbach[4] in 1958 in the context of a generalized optical potential, but it was usually omitted in phenomenological parametrizations of scattering data. During the last few years, the quality and scope of neutron scattering data has improved to such an extent that a careful examination of dispersion corrections has become possible and necessary.

Mahaux and co-workers have considered the problem of dispersion corrections in detail. (See Refs. 5–10 and references cited therein.) They argue (i) that the real part of the optical potential $V(r,E)$ at positive energy should connect smoothly, but nontrivially, to the shell model at negative energies through the dispersion correction, (ii) that more detailed information about $V(r,E)$ can be obtained from the study of differential and polarization cross sections at positive energy than from the study of bound state properties, and (iii) that an improved understanding of the shell model potential can be obtained by extrapolation of the scattering potentials to negative energy via the dispersion correction. Successful completion of such a program would not only unify the description of scattering data over a wide range of energies but would also provide a completely independent determination of absolute spectroscopic factors for bound quasiparticle states that could be compared with recent results from inelastic electron scattering and $(e,e'p)$ reactions.[11,12]

The accuracy with which the optical potential can be extrapolated to negative energy is a sensitive function of the phenomenological potential parameters that are used as input to the dispersion calculation. Mahaux and Sartor have emphasized the need for an improved analysis of scattering data particularly for $p+^{208}$Pb,[7,8] and the present work is intended to meet that need. In Sec. II we review some basic results of dispersion theory and present a critical examination of the existing data and previous analyses of the $p+^{208}$Pb and $n+^{208}$Pb potentials. Section III describes three different approaches to the problem of phenomenological potentials, and Sec. IV contains new results for the magnitude and energy dependence of the dispersion correction. The approach is unmistakably empirical, but considerable care is needed at just this point if the full potentialities of the dispersion theory approach are to be realized.

II. THE DISPERSION RELATION APPROACH

Following Mahaux and Sartor,[9] the real part of the mean field is written

$$V(r,E)=V_{\rm HF}(r,E)+\Delta V(r,E)\ , \tag{1}$$

where $V_{\rm HF}(r,E)$ is a Hartree-Fock–type contribution whose energy dependence is expected to be smooth. $\Delta V(r,E)$ is the dispersive contribution that is obtained from the imaginary part of the optical model potential by

the dispersion integral

$$\Delta V(r,E)=\frac{P}{\pi}\int_{-\infty}^{\infty}\frac{W(r,E')}{E'-E}dE' , \quad (2)$$

where P indicates a principal value. Moreover, the radial moments of the dispersive contribution are related to the corresponding moments of the imaginary potential by

$$[r^q]_{\Delta V}(E)=\frac{P}{\pi}\int_{-\infty}^{\infty}\frac{[r^q]_W(E')dE'}{E-E'} , \quad (3)$$

where

$$[r^q]_W(E)=\frac{4\pi}{A}\int_0^{\infty}W(r,E)r^q dr .$$

When $W(r,E')$ changes rapidly with energy as new channels open near the Fermi energy and new target excitations are possible, $\Delta V(r,E)$ can be substantial. At low energy $\Delta V(r,E)$ has the form of a surface-peaked potential which, when added to $V_{HF}(r,E)$, results in an energy-dependent geometry for the real, central potential, $V(r,E)$. The resulting rapid change in the real part of the potential, $V(r,E)$, at low energy has been called the Fermi energy anomaly. It is an anomaly in the sense that it is a departure from earlier phenomenological descriptions, but, in principle, it is a necessary correction for the finite probability that the target does not remain in its ground state during the elastic scattering process.

A similar effect has been observed in the elastic scattering of heavy ions near the Coulomb barrier.[13,14] As the bombarding energy approaches the Coulomb barrier from above, the empirical imaginary potential decreases sharply since nonelastic channels are effectively closed by the barrier. A corresponding increase in the depth of the real potential and an increase in the cross section for sub-barrier fusion are both described by a dispersion integral over the rapidly varying imaginary potential. (More recent analysis[14] suggests that the decrease in absorption at a given radial distance is due to a decrease in the radial extent of $W(r,E)$, i.e., an energy-dependent geometrical effect.)

Evaluation of $\Delta V(r,E)$ for nucleon scattering requires knowledge of $W(r,E')$ over the entire energy range $-\infty$ to $+\infty$, even though, in practice, phenomenological analysis of scattering data provides less than perfect knowledge of $W(r,E')$ over the energy range from a few MeV to at most a few hundred MeV. We follow the usual practice[5–10] that the imaginary potential at negative energy can be described by symmetry, i.e., $W(r,E_F+E')=W(r,E_F-E')$, where E_F is the Fermi energy.

The method has been applied to the $n+{}^{208}$Pb system using two different prescriptions. Mahaux and Sartor[9] represent the energy-dependent imaginary potential in terms of three radial moments, calculate the dispersive correction for each moment and reconstruct the central real potential from these calculated moments. Johnson, Horen, and Mahaux[15] represent the energy dependence of the imaginary potential with a volume absorption term (Woods-Saxon form) and a surface absorption term (derivative Woods-Saxon), each with a constant geometry but with energy-dependent depths. Their final real potential consists of three terms: a volume Woods-Saxon component that varies smoothly with energy, a volume Woods-Saxon term derived from a dispersion integral over the imaginary volume potential, and a surface component with energy dependence obtained from the dispersion integral over the surface imaginary component. Both methods require detailed information about the phenomenological imaginary potential $W(r,E')$. Since this information is available, both methods provide a good description of the $n+{}^{208}$Pb scattering over a wide range of positive energies, and both provide a suitable basis for extrapolation of the mean field to negative energies.

The situation for $p+{}^{208}$Pb is considerably less satisfactory.[7,8] One reason for this is that the extrapolation from positive to negative energy covers a considerably greater energy range for protons than for neutrons. The Coulomb barrier for protons ($\sim$16 MeV for ^{208}Pb) masks the nuclear potential below this energy, while for neutrons very accurate determinations of the nuclear potential have already been carried out down to 4 MeV.[2] Moreover, the presence of isobaric analog resonances complicates the energy dependence of the proton optical potential in the range 14 MeV $< E_p <$ 20 MeV. Another source of difficulty in the $p+{}^{208}$Pb case is the lack of consistency in previous analyses of proton scattering. This lack of consistency must now be considered briefly before we introduce the present analysis.

In their detailed treatment of dispersion effects in $n+{}^{208}$Pb, Johnson *et al.*[15] based all calculations on fits to the original measurements of total cross sections, differential elastic scattering cross sections, and analyzing power. By contrast, Mahaux and Sartor[6–10] started with optical model potential parameters from a wide variety of sources. They discussed the sensitivity of the results to the selection of starting values. One issue was whether or not the original authors allowed the geometrical parameters to vary in their calculations. A second criterion was the "goodness of fit" as assigned by Perey and Perey[16] in their compilation of published optical potentials. For neutron scattering, the procedure worked fairly well since most of the measurements were of recent vintage. In Ref. 9 their selection of neutron potentials was enhanced by a set of individual best fit calculations of Johnson which met all of the Mahaux-Sartor criteria for acceptable potentials.

For proton scattering, the tabulated potentials were based on analyses spread over many years. Some of the potentials were based on assumptions that are now considered implausible, while others imposed various constraints (e.g., constant geometry for the real part of the potential) that could mask the very effects of interest in the present application. The choice was then either to include questionable potentials or to apply the criteria discussed above strictly and thus reduce the input data available for the dispersion calculations. When the strict criteria were applied, all of the data below $E_p=20$ MeV were excluded except one set at 16 MeV, and that energy lay very close to the isobaric analog resonances at 15.6 and 16.3 MeV.[17] Dispersion calculations based on the re-

stricted set of potentials (but including the 16-MeV results) yielded very strong energy dependences for the moments and the ratios of the moments of the real potential. Extrapolation to negative energy lacked the stability that was obtained for neutron scattering. At least two reasons for this difficulty suggest themselves: (i) The energy range of the extrapolation is much larger for the $p+^{208}$Pb case than for the $n+^{208}$Pb case, and (ii) the extrapolation of the proton potential is strongly influenced by the least well determined point in the data set, i.e., the potential at 16 MeV, where isobaric analog resonances cannot be ignored. In view of the apparent success of the dispersion method for $n+^{208}$Pb, the very large effort thus far invested in the method, and the unsatisfactory condition of the $p+^{208}$Pb calculations, the need for a new analysis of the $p+^{208}$Pb potential is clear.

III. PHENOMENOLOGICAL ANALYSIS

In this section we describe three separate approaches to the determination of a suitable empirical optical potential for the $p+^{208}$Pb system. Since some of these methods are unconventional, a parallel analysis of the $n+^{208}$Pb system was conducted at each stage both as a control on the $p+^{208}$Pb analysis and as an extension of the work reported by Finlay and Petler.[3] The three approaches are conveniently described as (1) individual best fits, (2) grid searches, and (3) Fourier-Bessel expansions. The data base for the present analysis consists of the following measurements. *Proton scattering*: Cross section and analyzing power data at 9, 10, 11, and 12 MeV (Ref. 18), cross sections and analyzing power at 13 and 14 MeV (Refs. 19 and 20), cross sections at 21, 24.1, 26.3, 30.5, 35, and 47.3 MeV (Ref. 21), and cross sections at 40 MeV (Ref. 22), 49.4 MeV (Ref. 23), and 61.4 MeV (Ref. 24). Analyzing power data at 30.5, 40.0, and 49.4 MeV were also included in the analysis. *Neutron scattering*: Cross section data at 4, 4.5, 5, 5.5, 6, 6.5, and 7 MeV (Ref. 2), 9, 11, and 25.7 MeV (Ref. 25), 20, 22, and 24 MeV (Ref. 1), and 30.3 and 40 MeV (Ref. 26).

The proton data set improves upon the set available to Mahaux and Sartor by including the detailed measurements of Ref. 18 at low energy and by deleting the data set at 16 MeV, which is too close to the isobaric analog states to permit analysis in terms of a one-channel optical potential.[17] The neutron data set is nearly the same as that used recently by Johnson, Horen, and Mahaux.[15]

In all of the calculations described below, it is, of course, the shape elastic scattering that is described in terms of the optical potential. Below $E_n=7$ MeV compound elastic scattering is not negligible and very careful corrections were applied to the measured data. The procedure was described in detail in Ref. 2.

A. Individual best fits

We define the empirical optical potential as

$$U(r,E)=-V_R F(r,R_R,a_R)-iW_V F(r,R_V,a_V) +i4W_D a_D \frac{d}{dr}F(r,R_D,a_D) +\mathbf{L}\cdot\sigma\left[\frac{\hbar}{mc}\right]^2 V_{\rm SO}\frac{1}{r}\frac{d}{dr}F(r,R_{\rm SO},a_{\rm SO}) , \quad (4)$$

where $R_x=r_x A^{1/3}$ and $F(r,R_x,a_x)$ is a form factor. The optical potential was assumed to have a Woods-Saxon form factor for the real central potential, both volume Woods-Saxon and surface derivative Woods-Saxon imaginary central potential, and a real derivative Woods-Saxon spin-orbit potential. The proton spin-orbit potential was held fixed at the values given by Becchetti and Greenlees.[27] The neutron individual best-fit calculations of Ref. 3 used the spin-orbit potential of Annand *et al.*,[2] so several supplemental calculations were performed to verify that the main results for the central real and imaginary potentials were not very sensitive to this choice of spin-orbit potential.

In multiparameter searches of this type, there is always some ambiguity over the division of the absorptive term between its surface and volume components. Preliminary calculations verified the observation of Van Oers *et al.*[21] that for proton energy below $\sim$30 MeV the volume absorption term in Eq. (4) was very small. Accordingly, in both the individual best-fit and the grid-search analysis, we set W_V(proton)=0 for $E_p<30$ MeV. For neutrons, volume absorption was found to be nonzero at somewhat lower energies, again in agreement with previous analyses.[1,2,9] Hence, we require W_V(neutron)=0 for $E_n<10$ MeV. With these constraints, the remaining parameters of the potential were searched using the computer program FOP (Ref. 28) until a best fit (in the sense of minimum χ^2) to the scattering data was achieved. Results are displayed as the solid symbols in Figs. 1–3 for the real and imaginary volume integrals per nucleon J_V/A and J_W/A and the rms radius $R_{\rm rms}$. These quantities correspond exactly with the quantities $[r^2]_V$, $[r^2]_W$, and $T_{4/2}$ of Ref. 7. Final values of the parameters are given in Tables I and II.

B. Grid searches

There are two familiar shortcomings to the individual best-fit analysis described above. First, it is possible (and was indeed observed in the present work) that the best fit to the data is obtained when one or more of the parameters takes on an unreasonable value. Second, because of the complexity of the multidimensional χ^2 space, it is difficult to assign an uncertainty to the final parameters. The grid-search method provides a partial answer to both of these problems. In the present search, grids were formed on those two parameters, r_R and a_D, that showed the most significant energy dependence in earlier work.[2] The real radius parameter $r_R=R_R A^{-1/3}$ was fixed at values between 1.13 and 1.34 fm (0.01 fm steps), and the surface diffusivity a_D was fixed at values between 0.1 and 0.8 (0.1 or 0.05 fm steps). Since a complete grid search at each energy requires a very large number of calculations, the following constraints were imposed: $W_V=0$ for $E_n<10$ MeV and for $E_p<30$ MeV (as before), whenever $W_V\neq 0$, the geometrical parameters r_V and a_V were held fixed at reasonable average values learned from the individual best fits, and the spin-orbit parameters were held fixed at the Becchetti-Greenlees values[27] for both protons and neutrons. At each grid point, the values of the remaining parameters (V_R,W_V,W_D,a_R,R_D) were

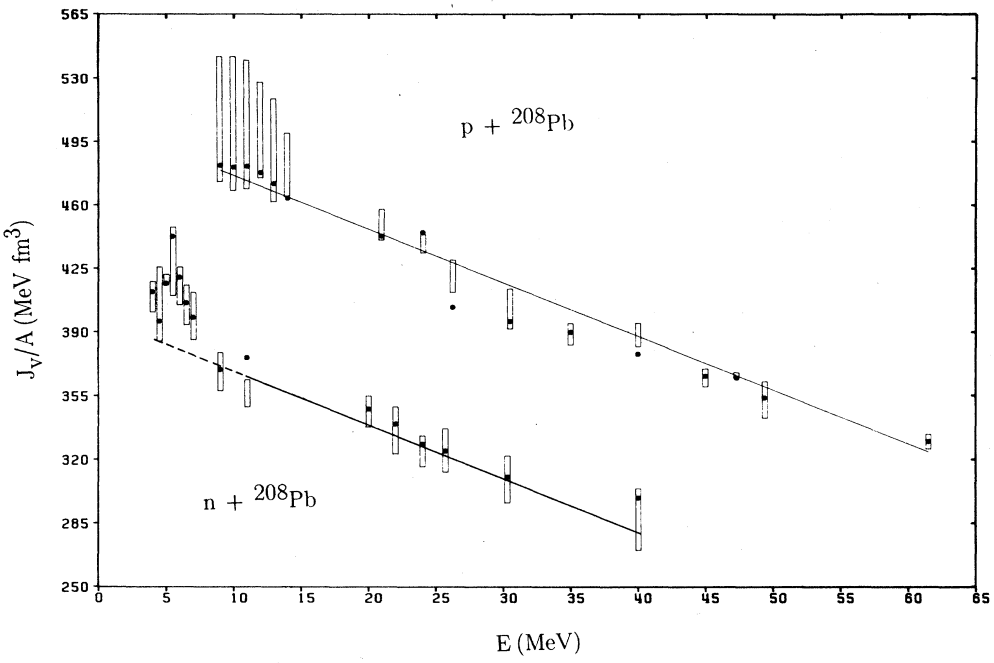

FIG. 1. Volume integral per nucleon versus energy for the real part of the potential for protons and neutrons and ^{208}Pb. The solid points are the results of individual best fits to the experimental data. The open bars are the limits of acceptability found for the grid searches as described in Sec. III. The line through the proton data is a least-squares fit to the grid-search results. A parallel line is drawn through the neutron data to guide the eye.

searched for best fit to the data at each energy. Final values of the remaining parameters were recorded for each search along with $\chi^2, J_V/A, J_W/A$ and $R_{\rm rms}$.

In most cases, a well-defined minimum in χ^2 could be located in the $r_R - a_D$ plane that could be used to determine some limits on the acceptability of parameter values. The method is not mathematically rigorous so we call the resulting range of parameter values "limits of acceptability" rather than error bars in the usual sense. The main goal of this grid-search exercise was to understand the reliability of the estimates of three quantities (J_V/A, J_W/A, and $R_{\rm rms}$) as determined directly from the measurements. The selection criteria for acceptable fits were as follows.

(1) χ^2 values no more than 50% larger than the minimum value were accepted at each energy.

(2) The radius parameter (r_D) of the surface absorption potential must be larger than the radius parameter (r_R) of the real central potential.

(3) The diffusivity of the real central potential a_R must

TABLE I. Individual best-fit parameters for the $p + ^{208}$Pb potential (energies in MeV, lengths in fm, $V_{SO} = 6.2$ MeV, $r_{SO} = 1.01$ fm, $a_{SO} = 0.75$ fm).

E_p	V_R	r_V	a_R	W_D	r_D	a_D	W_V	r_V	a_V
9	64.0	1.17	0.78	7.0	1.40	0.66	0		
10	64.2	1.17	0.77	7.7	1.30	0.69	0		
11	64.2	1.17	0.75	6.7	1.25	0.67	0		
12	63.3	1.17	0.75	6.7	1.25	0.66	0		
13	63.1	1.17	0.75	8.1	1.24	0.65	0		
14	61.9	1.17	0.76	7.4	1.29	0.66	0		
21	54.6	1.20	0.78	10.4	1.32	0.65	0		
24.1	52.9	1.22	0.71	10.3	1.23	0.77	0		
26.3	52.9	1.19	0.65	7.7	1.34	0.87	0		
30.5	51.3	1.18	0.75	9.1	1.25	0.71	4.3	1.06	0.79
35	48.6	1.21	0.63	5.1	1.20	0.84	3.2	1.34	0.72
40	52.5	1.14	0.83	4.7	1.33	0.76	4.3	1.32	0.66
45	49.6	1.17	0.72	6.3	1.24	0.74	3.2	1.24	0.74
47.3	49.2	1.17	0.74	6.5	1.24	0.73	3.6	1.19	0.70
49.4	46.6	1.18	0.72	5.6	1.27	0.70	4.0	1.18	0.72
61.4	43.1	1.20	0.59	6.6	1.25	0.73	2.2	1.34	0.73

be less than 0.8 fm.

(4) The radius parameter (r_D) of the surface absorption term may not exceed 1.40 fm.

The first criterion is entirely arbitrary but appropriate for the present purpose, i.e., to explore the limits of acceptability of the parameter values that provide a good description of the data. The consequences of allowing a 50% degradation in χ^2 are illustrated in Fig. 4(a) for 12-MeV protons and in Fig. 4(b) for 7-MeV neutrons. It is clear from Fig. 4 that the calculations with larger χ^2 also provide a very good description of the data. The second criterion codifies a property of almost all optical models in the literature and is a property of optical potentials obtained from microscopic folding models. It is discussed at some length in Ref. 29. The third and fourth criteria are also consistent with the history of optical model studies.

Results of the grid searches are listed in Tables III and IV and shown as open bars in Figs. 1–3. For the most part, the individual best fits fall within the range of ac-

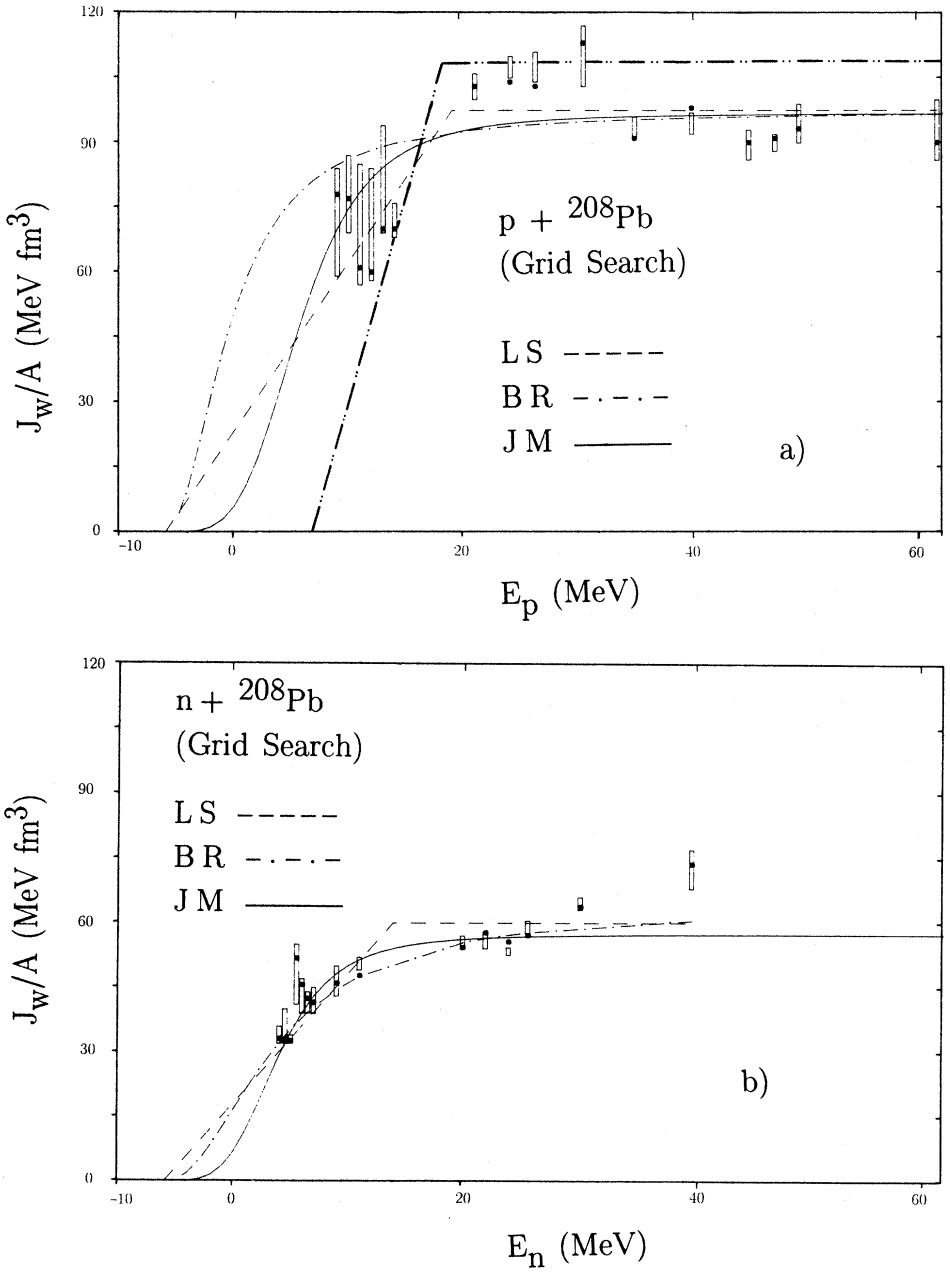

FIG. 2. Volume integral per nucleon versus energy for the imaginary part of the potential for (a) protons and (b) neutrons and ^{208}Pb. The solid points and open bars were defined in Fig. 1. The lines through the data are best fits of the grid-search results to analytic functions discussed in Sec. IV. The dash-dot-dot-dash line is redrawn from Ref. 7.

TABLE II. Individual best fit parameters for the $n + {}^{208}Pb$ potential (energies in MeV, lengths in fm, $V_{SO} = 5.75$ MeV, $r_{SO} = 1.105$ fm, $a_{SO} = 0.499$ fm).

E_n	V_R	r_V	a_R	W_D	r_D	a_D	W_V	r_V[a]	a_V[a]
4.0	45.4	1.29	0.63	6.7	1.27	0.36			
4.5	47.6	1.21	0.83	14.5	1.35	0.15			
5.0	43.9	1.28	0.73	16.7	1.35	0.13			
5.5	41.0	1.33	0.74	13.5	1.38	0.24			
6.0	42.2	1.29	0.75	15.2	1.38	0.19			
6.5	43.2	1.27	0.70	10.4	1.34	0.27			
7.0	44.0	1.26	0.70	8.8	1.32	0.31			
9.0	45.9	1.20	0.76	6.6	1.32	0.47			
11.0	42.9	1.25	0.65	5.5	1.20	0.69	<0.2	1.20	0.69
20.0	43.6	1.20	0.71	5.7	1.23	0.58	1.45	1.23	0.58
22.0	44.3	1.18	0.71	5.0	1.29	0.52	2.19	1.29	0.52
24.0	44.5	1.17	0.71	4.4	1.29	0.55	2.16	1.29	0.55
25.7	43.1	1.18	0.70	4.8	1.24	0.66	1.84	1.24	0.66
30.3	43.3	1.16	0.71	3.7	1.31	0.55	3.33	1.31	0.55
40.0	38.9	1.18	0.76	2.6	1.32	0.49	5.47	1.32	0.49

[a] $r_V = r_D$, $a_V = a_D$ as in Ref. 3.

ceptability, but when they do not it is usually because one of the above criteria was violated in the free, individual best-fit searches. The case of neutron scattering at 40 MeV is perhaps the most interesting since it showed a clear double minimum in χ^2 space—both of which have been previously reported in the literature.[1,9] These minima occur at values of r_R of ≈ 1.13 and 1.25. In the present analysis, the minimum at $r_R \simeq 1.25$ is excluded by criterion 2 ($r_D > r_R$). The resulting solution for smaller r_R is much more consistent with the general trends in the data, and its use would serve to remove a difficulty in a

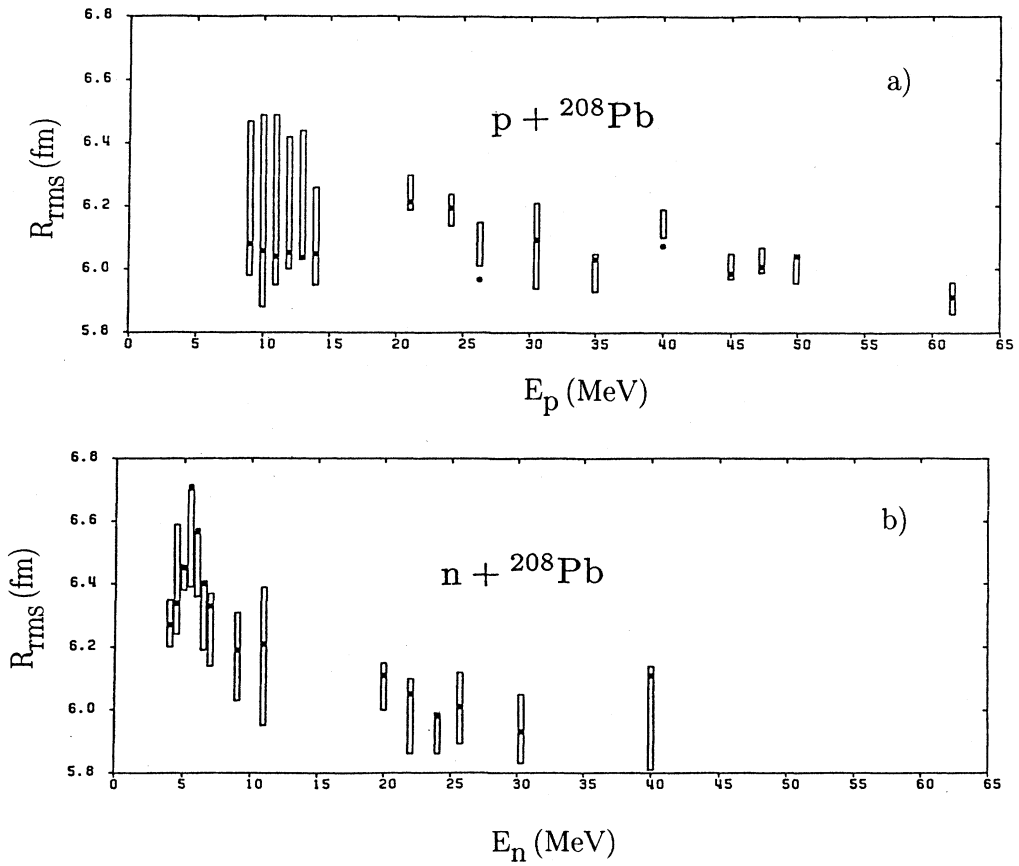

FIG. 3. Root-mean-square radius of the real part of the optical potential versus energy for (a) protons and (b) neutrons and ^{208}Pb. The solid points and open bars have the same meaning as in Fig. 1.

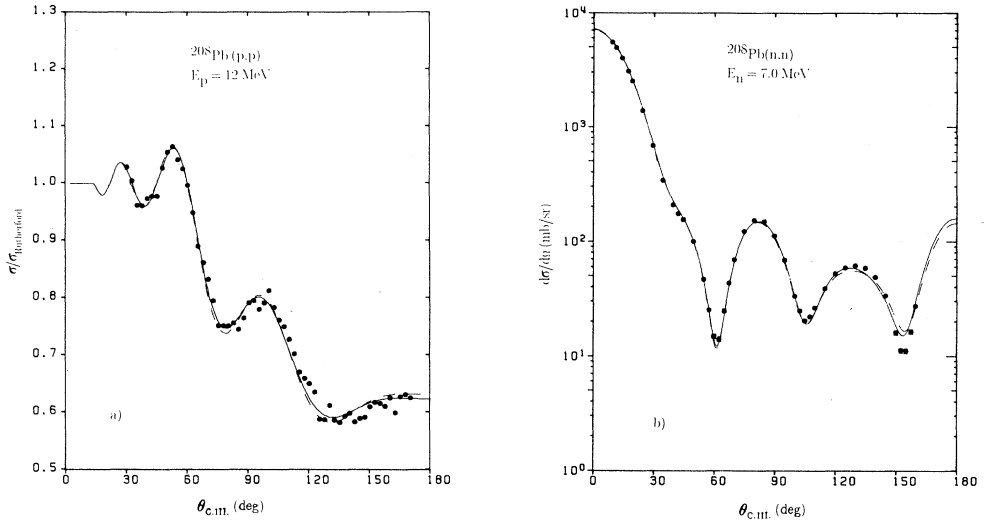

FIG. 4. Optimum fit to the differential cross section data from the grid search (solid lines) for scattering of (a) 12-MeV protons and (b) 7-MeV neutrons from ^{208}Pb. The dashed lines in each case show the slightly degraded fits that result from optical parameters that lead to χ^2 values 50% higher than the optimum results.

recent application of the moment method.[9]

Analysis of the proton scattering data below 12 MeV provides a clear illustration of the value of the grid-search approach. At these energies the Coulomb potential tends to mask the nuclear potential. Differential cross sections show only weak diffraction patterns and analyzing powers are small ($<3\%$). Thus, in spite of the excellent quality of the data, a very wide range of optical model parameters provides satisfactory fits to the data. (The χ^2 valley was so flat that the criterion of a 50% increase in χ^2 was never achieved at 9–11 MeV.) Application of criteria (2)–(4) led to some limitation on the range of the parameters, but eventually, a new constraint was required. The radius parameter of the surface imaginary term, r_D, was held fixed at a series of values (1.28, 1.295, and 1.32 fm) taken from widely used "global" optical models.[30,31,27] As before, a grid on the parameters r_R and a_D was constructed, and the remaining parameters were varied for each grid point until a best fit to the data was obtained. Final values for the range of J_V/A, J_W/A, and $R_{\rm rms}$ were obtained by combining the results from the calculations at the three fixed values of r_D.

Several qualitative features of the individual best-fit and grid-search procedures can be seen from an examination of Figs. 1–3.

(1) The limits of acceptability of the parameters of the optical model are quite broad for low-energy (<15 MeV) protons and quite narrow for high-energy protons. The neutron-nucleus potential is determined better than the proton potential at low energy but less well at high ener-

TABLE III. Volume integrals (in MeV fm^3) and root-mean-square radii (in fm) for $p+^{208}$Pb.

	Individual best fits			Grid searches					
				J_V/A		J_W/A		$R_{\rm rms}$	
E_p	J_V/A	J_W/A	$R_{\rm rms}$	min	max	min	max	min	max
9	482	78	6.08	473	542	59	84	5.98	6.47
10	481	77	6.06	468	542	69	87	5.88	6.49
11	481	61	6.04	469	540	57	85	5.95	6.49
12	478	60	6.05	475	528	58	84	6.00	6.42
13	472	70	6.04	462	519	69	94	6.03	6.44
14	464	70	6.05	465	500	68	76	5.95	6.26
21	443	103	6.22	441	458	100	106	6.19	6.30
24.1	445	104	6.20	434	444	105	110	6.14	6.24
26.3	404	103	5.97	412	430	104	111	6.01	6.15
30.5	396	113	6.09	392	414	103	117	5.94	6.21
35	390	91	6.03	383	395	91	96	5.93	6.05
40	378	98	6.07	382	398	92	97	6.10	6.19
45	366	90	5.99	360	370	86	93	5.97	6.05
47.3	365	91	6.01	365	368	88	92	5.99	6.07
49.4	351	93	6.04	343	365	90	99	5.96	6.04
61.4	330	90	5.91	326	334	86	100	5.86	5.96

TABLE IV. Volume integrals (in MeV fm^3) and root-mean-square radii (in fm) for $n + {}^{208}$Pb.

	Individual best fits			Grid searches					
				J_V/A		J_W/A		R_{rms}	
E_n	J_V/A	J_W/A	R_{rms}	min	max	min	max	min	max
4	412	33	6.27	401	418	32	36	6.20	6.35
4.5	396	33	6.34	385	426	32	40	6.24	6.59
5	417	33	6.45	416	422	32	34	6.38	6.46
5.5	443	52	6.71	410	448	41	55	6.39	6.70
6	420	46	6.57	405	426	39	47	6.36	6.56
6.5	400	42	6.40	394	416	39	44	6.19	6.41
7	398	41.51	6.33	386	412	39	45	6.14	6.37
9	370	46	6.18	358	379	43	50	6.03	6.31
11	376	48	6.21	349	364	49	52	5.95	6.39
20	348	54	6.11	338	355	54	57	6.00	6.15
22	339	58	6.05	323	349	54	58	5.86	6.10
24	328	56	5.98	316	333	53	54	5.86	5.99
25.7	325	57	6.01	313	337	58	61	5.89	6.12
30.3	310	64	5.93	296	322	63	66	5.83	6.05
40	299	74	6.11	270	304	68	77	5.81	6.14

gy.

(2) The real volume integral for protons is well described as a linear function of energy over the entire range of the data. The solid line in Fig. 1 is a least-squares fit to the grid search results (treating the range of acceptability now as a mean value and an uncertainty) yielding

$$J_V/A = (504.5 \pm 5.9) - (2.92 \pm 0.13)E \ (\text{MeV fm}^3) \ .$$

Because of their large ranges of acceptability, the points below $E_p = 14$ MeV have little influence on the slope of the line. At the same time, a significant rise in the volume integral at $E_p < 14$ MeV is consistent with the results of the grid search. Interestingly, the individual best-fit results are well described by the straight line the slope of which is in excellent agreement with global optical potentials.[32] Such a result would be inexplicable in terms of dispersion corrections. This observation (Fig. 1) provides the strongest testimony for the importance of parameter uncertainty considerations in optical model analysis.

(3) The trend in J_V/A for neutrons, however, is well described by a parallel straight line (Fig. 1) for $E > 10$ MeV and a narrow region of enhancement for $E < 7$ MeV.

(4) The energy dependence of J_W/A (Fig. 2) is roughly similar for neutrons and protons near threshold. More detailed comparisons will be performed in Sec. IV, where dispersion calculations are discussed. For now it is important to observe that the present analysis excludes the dash-dot-dot-dash line that was used to represent $J_W(E)/A$ for protons in Ref. 7. We refer to models for $J_W(E)/A$ that intercept the positive energy axis as Coulomb cutoff models and return to them in Secs. IV and V.

(5) The rms radius of the real proton potential (Fig. 3) shows only a slight tendency to decrease with increasing energy, while the rms radius of the neutron potential shows a sharp enhancement for $E < 10$ MeV.

(6) Both for the individual best fits and for the grid searches, χ^2 was minimized for values of the surface diffusivity $a_D > 0.60$ fm for protons at every energy, while for neutrons all of the data below ≈ 7 MeV required $a_D < 0.40$ fm.

Observations (2) and (5) contain some of the main results of the present work. They are in contrast with an earlier phenomenological analysis[19] of $p + {}^{208}$Pb scattering where evidence of a rapid change in slope of $V(r,E)$ near the Coulomb barrier was obtained in the framework of a fixed-geometry model and with a less complete data set. The present results contrast even more sharply with the dispersion relation calculations of Mahaux and Sartor in Ref. 7, where rapid excursions in both $J_V(E)/A$ and R_{rms} were predicted at 15 MeV $< E_p <$ 30 MeV. On the other hand, a more recent dispersion analysis by these authors[10] is in overall agreement with our new results in that the anomaly in $J_V(E)/A$ is no longer visible in the energy domain $E_p > 15$ MeV, and the energy dependence of R_{rms} is much gentler than in the earlier work. The differences between Refs.7 and 10 are clearly important in the present context and will be discussed in Sec. IV.

Observation (6) is a less obvious but perhaps interesting feature of the analysis. The tendency of the surface imaginary diffuseness to decrease with decreasing energy was noted by Annand *et al.*[2] in their analysis of $n + {}^{208}$Pb and ^{209}Bi and strongly confirmed by Lawson, Guenther, and Smith in an independent study of $n + {}^{209}$Bi (Ref. 33) and for $n + {}^{89}$Y (Ref. 34). The effect was anticipated by Moldauer[35] in a study of s-wave strength functions and scattering data at very low energy. If a decrease in a_D at low energy is a phenomenological hallmark of the strong surface coupling that characterizes the Fermi energy anomaly, it appears that the most interesting region for $p + {}^{208}$Pb has not been reached for $E_p > 9$ MeV (see Tables I and II).

C. Fourier-Bessel expansions

The large uncertainty in the values of optical model parameters is one of the noteworthy results of the grid

search analysis. Can these uncertainties be reduced? In this section we attempt to extract the features of the real and imaginary potentials directly from the data without constraining the analysis to the conventional Woods-Saxon form factors. The method consists of adding to the Woods-Saxon potential an extra term given by a Fourier-Bessel series, e.g.,

$$V(r)=\frac{V_R}{1+e^x}-\sum_{n=1}^{N} b_n j_0(q_n r) , \tag{5}$$

where

$$x=(r-r_R A^{1/3})/a_R . \tag{6}$$

The j_0 are spherical Bessel functions and $q_n=n\pi/R$, where R is a cutoff radius. The computer code GENOA (Ref. 36) has been modified to search on the b_n's for best fit to the data. By introducing a matrix inversion routine into GENOA, the covariance matrix M of the parameters b_n may be obtained from the secular equations that minimize χ^2/N. The diagonal elements of the matrix M are the errors in the coefficients b_n, and the correlations between them are given by the off-diagonal elements. With these quantities, one can construct a much better statement of the uncertainties in the quantities of interest, i.e., J_V/A and $R_{\rm rms}$. A similar expansion can be carried out simultaneously for the imaginary potential with appropriate modifications in the error matrix.

In the present work, Fourier-Bessel expansions were performed simultaneously for both the real and imaginary potentials (an extension of the work of Ref. 3). In most cases, good convergence was obtained at a large enough cutoff radius (12 fm) to justify the claim of model independence. Minimization of the quantity χ^2 per degree of freedom was strictly observed in order to study the number of terms in the expansion required to obtain an optimal description of the scattering data. Once again, proton scattering near the Coulomb barrier provided the most difficult fitting problem.

Results from the Fourier-Bessel expansion analysis are summarized in Fig. 5 for the volume integral of the real potential and in Fig. 6 for the volume integral of the imaginary potential. Comparison of Figs. 5 and 6 with Figs. 1 and 2, respectively, shows that all of the trends observed in the results of the grid searches are also observed in the Fourier-Bessel analysis: (a) real volume integrals show an enhancement for low-energy neutrons but not for low-energy protons, (b) the imaginary volume integrals have similar threshold behavior for protons and neutrons, and (c) uncertainties in the volume integrals for the proton potential are somewhat smaller in the Fourier-Bessel analysis than in the grid search. This suggests that the 50% change in the χ^2 criteria used in the grid searches was a bit too generous for the proton data. The reduced uncertainty at low proton energy is a direct result of the inclusion of the excellent low-energy analyzing power data of Ref. 18. An earlier report of the present work[37] mentioned huge uncertainties in the Fourier-Bessel imaginary potential, but those results were obtained before the analyzing power data had been incorporated into the analysis.

We conclude that the three phenomenological analyses are in good general agreement on the energy dependence of the real and imaginary parts of the ^{208}Pb optical potential for protons and neutrons. We turn now to dispersion

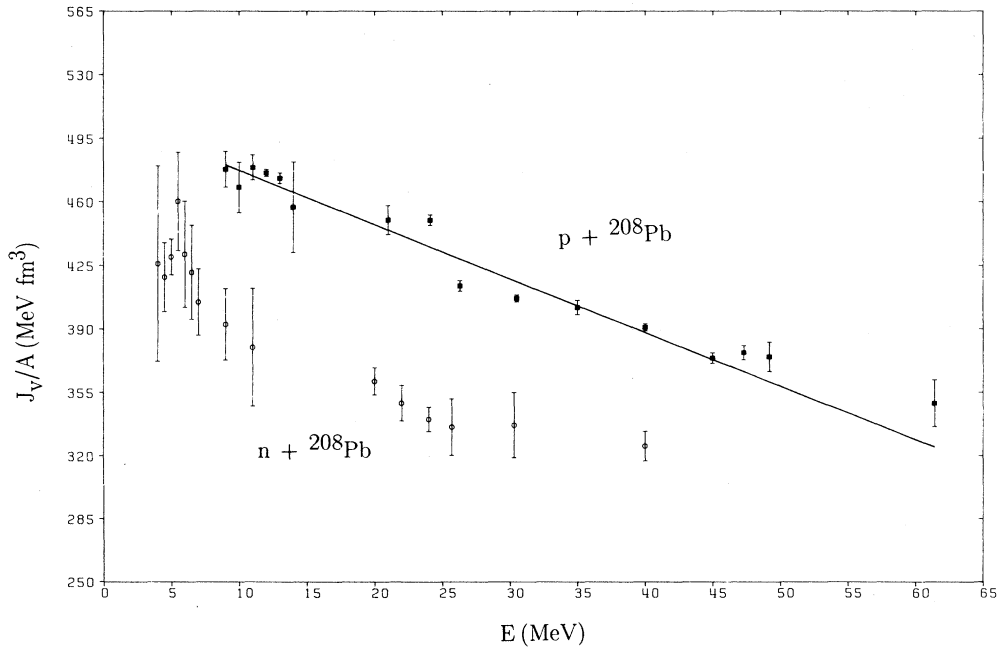

FIG. 5. Fourier-Bessel analysis results for the volume integral per nucleon versus energy of the real part of the potential for protons (solid squares) and neutrons (open circles) and ^{208}Pb. The solid line through the proton data is taken directly from Fig. 1 to facilitate comparison with the grid-search results.

relations for an understanding of this new phenomenology.

IV. DISPERSION CALCULATIONS

In order to carry out the dispersion integral [Eq. (2)], a functional representation of J_W/A vs E is required. Three specific forms have been recently advanced by Mahaux and Sartor.[7,9] (1) The linear segment (LS) form is given simply by

$$J_W(E)/A = l\frac{(E-E_F)}{(s-E_F)}, \quad E_F \le E \le s$$
$$= l, \quad E \ge s \ .$$

(2) The Brown-Rho[38] (BR) form is given by

$$J_W(E)/A = b\frac{(E-E_F)^2}{(E-E_F)^2+r^2} \ .$$

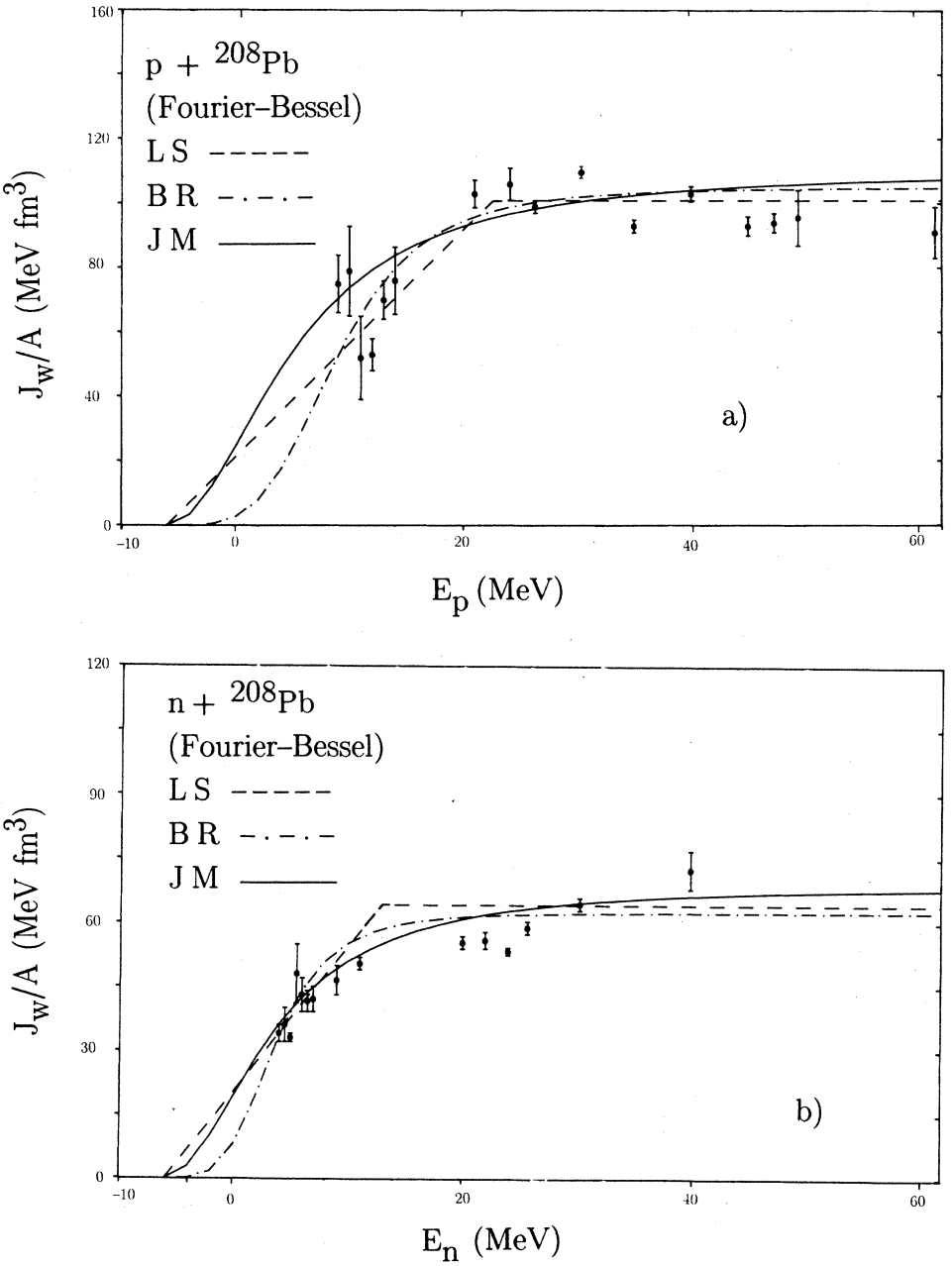

FIG. 6. Fourier-Bessel analysis results for the volume integral per nucleon of the imaginary part of the potential for (a) protons and (b) neutrons and ^{208}Pb. The lines through the data are best fits of the Fourier-Bessel results to the analytic functions discussed in Sec. IV.

(3) The Jeukenne-Mahaux[39] (JM) form is given by

$$J_W(E)/A = j\frac{(E-E_F)^4}{(E-E_F)^4+m^4} .$$

Each of these three parametric forms was fitted to the grid-search parameters and to the Fourier-Bessel expansion parameters. The best fits are shown as lines in Figs. 2 and 6, and the resulting parameter values are given in Table V. It should be noted that the fits to the proton data for J_W/A show more scatter than the corresponding fits to the neutron data.

With these parametrizations of J_W/A, the dispersion integral can be evaluated either numerically or analytically for the dispersion correction to the real, central volume integral. (By limiting this calculation to volume integrals, we avoid the need to determine separate energy dependences for the surface and volume absorption terms in the phenomenological model.) The calculated quantity is the sum of the polarization (J_{PO}) and correlation (J_{CO}) contributions[5] to the total volume integral. Typical results are shown in Fig. 7. There are twelve such dispersion calculations to evaluate (three fitting functions and two kinds of nucleons for both the grid search and the Fourier-Bessel optical parameters). In Fig. 7 we show results for the JM parametrization that seems to provide the best overall representation of the data in Figs. 2 and 6; dispersion corrections calculated with the other parametric forms are similar in shape. The differences in detail, however, can be informative. We characterize each calculation of $\Delta J = J_{PO} + J_{CO}$ in terms of two parameters: The maximum amplitude of the correction (ΔJ^{max}) and the incident energy at which the correction is a maximum (E^{max}). The amplitude of the correction is proportional to the product of the parameters br (jm) for the BR (JM) parametrizations, respectively, and has extrema at $E-E_F=\pm r(m)$. Since b (j) is the value of the imaginary volume integral for $E \gg E_F$, it is automatically larger for protons than for neutrons because the Coulomb correction and the symmetry term in the potential increase proton absorption for $N>Z$ nuclei. Values of these parameters are given in Table VI. Note that the abscissa in Fig. 7 is $E-E_F$, where E_F (the Fermi energy) is -6 MeV, while E_n, E_p, and E^{max} are projectile energies in the laboratory.

Examination of Table VI shows that the scatter in the calculated dispersion correction is significantly greater for protons than for neutrons, i.e., 0 MeV $< E_p^{max} <$ 14.5 MeV, while 3.5 MeV $< E_n^{max} <$ 8 MeV. The present results for ΔJ for neutrons are all in approximate agreement with the recent LS (Ref. 7) and BR and JM (Ref. 9) parametrizations by Mahaux and Sartor both in the magnitude of the correction and in the energy (E_n^{max}) at which the maximum correction occurs. The origin of this good agreement is found in the similarity of the parameters used to describe the energy dependence of J_W/A, and this similarity is a direct result of using nearly the same neutron potential parameters for both analyses.

For proton scattering, the situation is less clear. The various parametrizations of J_W/A differ significantly from one another in the important region below $E_p=9$ MeV, where there are no data to constrain the functions. Moreover, the uncertainties in the values of J_W/A for protons are relatively large below $E_p \simeq 20$ MeV. The scatter in the calculated values of ΔJ and E_p^{max} (Table II) can be attributed directly to these two effects, i.e., lack of data below 9 MeV and larger parameter uncertainty below 20 MeV. Even so, the *average* behavior of ΔJ_p is quite similar to the *average* behavior of ΔJ_n. If the LS parametrization is excluded on the grounds that a sudden change in the slope of $J_W(E)/A$ is unphysical, the shape of the predicted ΔJ vs E is practically the same for protons and neutrons; specifically, the incident energy at which the dispersion correction is a maximum is in the neighborhood of 3–5 MeV for both neutrons and protons.

This last observation is quite different from our expectations if the presence of the Coulomb barrier served to cut off the imaginary potential for low-energy protons. One calculation,[7] which incorporated such a Coulomb cutoff effect by letting the proton imaginary potential go to zero at $E_p \sim +7$ MeV, yielded a very large dispersion correction ($\Delta J^{max}=98$ MeV fm^3, $E_p^{max}=14$ MeV). We find no support for such a result in the present analysis. The trend of the present empirical values of J_W/A vs E for protons is not very different from the trend for neutrons. Moreover, a correction of such large amplitude peaking at $E_p=14$ MeV would likely produce observable consequences in the present empirical values of J_V/A for protons, but no such effects are visible in Figs. 1 and 5. We note that the reanalysis of $p+^{208}$Pb of Ref. 10 does not employ a Coulomb cutoff in $J_W(E)/A$ [the BR and JM forms are used and $J_W(E)/A \to 0$ at $E=E_F$], and the resulting moments for the full real potential reach their maxima at energies below the Coulomb barrier.

Finally, we comment briefly on the differences between the dispersion calculations of Refs. 7 and 10. Reference 10 appeared while the present work was already in progress. The improvements that result from the removal of a Coulomb cutoff have already been emphasized. Another significant improvement was the incorporation of po-

TABLE V. Parameters used to fit the energy dependence of the volume integral of the imaginary part of the potential.

	l	s	b	r	j	m
Proton grid search	97.5	19.3	97.2	5.7	96.7	11.8
Proton Fourier-Bessel	101	22.6	110.5	11.3	105.1	15
Neutron grid search	60	13.9	63	9.5	57.4	9.9
Neutron Fourier-Bessel	64.3	12.9	69.4	9.6	62.6	9.7

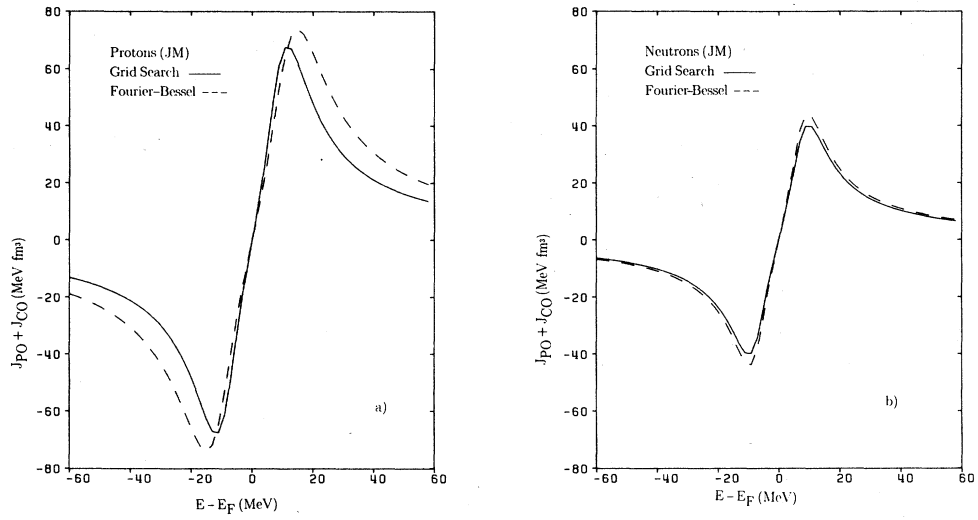

FIG. 7. The dispersion correction to the volume integral per nucleon of the real part of the potential for (a) protons and (b) neutrons vs $E - E_F$, where E_F ($= -6$ MeV) is the Fermi energy. All curves are calculated with the JM fitting function of Sec. IV. The solid lines are based on the grid-search results of Fig. 2 and the dashed lines are based on the Fourier-Bessel results of Fig. 6.

tential parameters at 16 MeV from an analysis that included isobaric analog resonances.[17] (We preferred to omit the region 14 MeV $< E_p <$ 20 MeV altogether.) Lastly, several optical model parameter sets from the tabulation of Perey and Perey[16] were added in the energy region 8 MeV $\leq E_p \leq$ 14 MeV. These parameter sets were helpful in reducing the range of extrapolation of the real potential, but they were also crucial in defining the energy dependences of the moments of the imaginary potential. The specific potentials selected below 14 MeV suffer from one or more of the defects discussed in the introduction. Their inclusion could distort the subsequent analysis for reasons that are now briefly discussed.

In many recent phenomenological analyses, the usual practice is to require a surface-peaked form factor at low energy and a gradual transition to a volume form factor as the energy is increased. For neutrons, the onset of volume absorption is typically found to be about 10–12 MeV.[2] For protons, there appears to be no need for a volume absorption term below about 30 MeV in either the present work or in the analysis by Van Oers *et al.*[21] This traditional representation of the energy dependence of the absorption is fully confirmed by the Fourier-Bessel analysis in Sec. III. A clear surface-volume mixture is obtained for the imaginary form factor by 22 MeV for neutrons and by 47 MeV for protons. The choice of a pure volume form factor for $p + {}^{208}$Pb below 14 MeV by Mo and Davis[40] is inconsistent with this well-established picture. Moreover, these low-energy potential parameters tend to distort the calculation of the moments of the imaginary potential and yield questionable results for the form factor and energy dependence of the dispersion correction to the real potential.

The present analysis of the low-energy proton cross section and analyzing power measurements by Kretschmer *et al.*[18] yields a much more reasonable representation of the optical potential. The large uncertainties simply reflect the difficulty in determining the $p + {}^{208}$Pb interaction below the Coulomb barrier. It seems appropriate to use these new results in a new analysis of the dispersion both with the moment method and with the method of Johnson *et al.*[15]

TABLE VI. Parameters characterizing the magnitude and shape of the dispersion correction $\Delta J = J_{PO} + J_{CO}$; ΔJ^{max} in MeV fm^3; E^{max} in MeV.

	Grid search		Fourier-Bessel	
	ΔJ^{max}	E^{max}	ΔJ^{max}	E^{max}
Protons				
LS	54.6	11.5	56.3	14.5
BR	48.5	−0.3	54.7	5.3
JM	68	5.8	74	9
Neutrons				
LS	33.6	8	35.9	7.4
BR	31.4	3.5	34.5	3.6
JM	40.4	3.9	44.1	3.7

V. CONCLUSIONS

A comprehensive examination of elastic scattering from ^{208}Pb has been performed below 61 MeV for both protons and neutrons. Reliable estimates of the values and the uncertainties of the derived quantities J_V/A, J_W/A, and R_{rms} are obtained because the analysis avoided the use of preconditions on the geometrical parameters. The limits of acceptability (or uncertainty) in many parameters are quite large for low-energy protons because of the masking effect of the Coulomb potential. Previously reported "anomalies" in the energy dependence of J_V/A and R_{rms} are confirmed for $n + {}^{208}$Pb but not confirmed for $p + {}^{208}$Pb in the available energy region.

An important conclusion may be drawn from the present analysis of proton and neutron scattering. The energy dependence of the imaginary potential is quite similar for both projectiles (see Figs. 2 and 6). In contrast to recent observations in heavy-ion elastic scattering, the Coulomb barrier does not cut off the imaginary potential in the $p+^{208}$Pb system. The phenomenology developed in this paper is consistent with the notion that the imaginary potential is dominated by damping into complex modes of the target-plus-projectile system, rather than by direct reaction channels that would indeed be closed off as the proton energy is lowered below the Coulomb barrier. We suggest, therefore, that the origin of the imaginary potential may be different for scattering of nucleons and heavy ions.

Dispersion models provide estimates of the corrections to the real potential that can be compared with the results of the phenomenological analysis. The neutron data (Fig. 1) are entirely consistent with the calculated dispersion correction of 30–40 MeV fm^3 peaking at about 4–5 MeV. The even larger predicted corrections to the proton data were not found either in the best-fit calculations or in the Fourier-Bessel expansions. However, an effect is suggested within the large uncertainties of the grid-search calculations below 14 MeV. This is not intended to suggest that the "Fermi energy anomaly" is absent for the proton potential. Indeed, if Fig. 1 were extended to negative energies to include the bound states (work in progress), a large departure from the straight line would definitely be required. Lawson *et al.*[33] made the same observation for $n+^{209}$Bi. We do conclude, however, that a consistent analysis of the scattering data alone was unable to find convincing evidence for what should be a large effect. The present analysis further suggests an explanation for this new result, namely that the dispersion correction for both neutrons and protons has its largest effect below $\sim$10 MeV, where, for protons, it would be exceedingly difficult to observe.

Although it would be very valuable to have more precise values for the proton potential parameters below the Coulomb barrier, the traditional study of cross section and analyzing power measurements seems to be reaching its limits. A careful measurement of total reaction cross section for $p+^{208}$Pb below 14 MeV might reduce the limits of acceptability of the proton potential parameters and thus provide firmer basis for extrapolating the optical potential to negative energy. Sub-barrier deuteron stripping reactions might provide another useful constraint on the potential.

ACKNOWLEDGMENTS

The authors wish to express their gratitude to J. McDougall for his assistance with the extensive computer calculations and helpful comments. The research was supported by the National Science Foundation (Grant No. PHY-8507137), by Ohio University, and by Lawrence Livermore National Laboratory (Contract No. W-7405-ENG48).

[1]R. W. Finlay, J. R. M. Annand, T. S. Cheema, J. Rapaport, and F. S. Dietrich, Phys. Rev. C **30**, 796 (1984).
[2]J. R. M. Annand, R. W. Finlay, and F. S. Dietrich, Nucl. Phys. **A443**, 249 (1985).
[3]R. W. Finlay and J. S. Petler, in *Use of the Optical Model for the Calculation of Neutron Cross Sections Below 20 MeV* (Organization for Economic Cooperation and Development, Paris, 1986), pp. 43–52.
[4]H. Feshbach, Ann. Phys. (N.Y.) **5**, 357 (1958).
[5]C. Mahaux and H. Ngô, Nucl. Phys. **A378**, 205 (1982).
[6]C. Mahaux and R. Sartor, Nucl. Phys. **A458**, 25 (1986).
[7]C. Mahaux and R. Sartor, Nucl. Phys. **A460**, 466 (1986).
[8]C. Mahaux and R. Sartor, Phys. Rev. C **34**, 2119 (1986).
[9]C. Mahaux and R. Sartor, Nucl. Phys. **A468**, 93 (1987).
[10]C. Mahaux and R. Sartor, Nucl. Phys. **A481**, 381 (1988).
[11]E. N. M. Quint *et al.*, Phys. Rev. Lett. **57**, 186 (1986).
[12]B. N. Frois and C. N. Papanicolas, Annu. Rev. Nucl. Part. Sci. **37**, 133 (1987).
[13]M. A. Nagarajan, C. C. Mahaux, and G. R. Satchler, Phys. Rev. Lett. **54**, 1136 (1985).
[14]C. Mahaux, H. Ngô, and G. R. Satchler, Nucl. Phys. **A449**, 354 (1986); **A456**, 134 (1986).
[15]C. H. Johnson, D. J. Horen, and C. Mahaux, Phys. Rev. C **36**, 2252 (1987).
[16]C. M. Perey and F. G. Perey, At. Data Nucl. Data Tables **17**, 1 (1976).
[17]R. Melzer, P. Von Brentano, and H. Paetz Gen. Scheck, Nucl. Phys. **A432**, 363 (1985).
[18]W. Kretschmer, M. Loh, K. Spitzer, and W. Stach, Phys. Lett. **87B**, 343 (1979); and private communication.
[19]J. S. Eck and W. J. Thompson, Nucl. Phys. **A237**, 83 (1975).
[20]R. D. Rathmell and W. Haeberli, Nucl. Phys. **A178**, 458 (1972).
[21]W. T. H. Van Oers *et al.*, Phys. Rev. C **10**, 307 (1974).
[22]M. P. Fricke, E. E. Gross, B. J. Morton, and A. Zucker, Phys. Rev. **156**, 1207 (1967).
[23]G. S. Mani, D. T. Jones, and D. Jacques, Nucl. Phys. **A165**, 384 (1971).
[24]C. B. Fulmer, J. B. Ball, A. Scott, and M. L. Whiten, Phys. Rev. **181**, 1565 (1969).
[25]D. E. Bainum, R. W. Finlay, J. Rapaport, J. D. Carlson, and W. G. Love, Phys. Rev. C **16**, 1377 (1977).
[26]R. DeVito, Ph.D. dissertation, Michigan State University, 1979; R. P. DeVito, S. M. Austin, U. E. P. Berg, and W. Sterrenburg, Michigan State Cyclotron Laboratory Report MSUCL-363, 1981.
[27]F. D. Becchetti, Jr. and G. W. Greenlees, Phys. Rev. **182**, 1190 (1969).
[28]F. S. Dietrich, computer code FOP (1983).
[29]P. E. Hodgson, *Nuclear Reactions and Nuclear Structure* (Clarendon, Oxford, 1971).
[30]R. L. Walter and P. O. Guss, *Proceedings of the International Conference on Nuclear Data for Basic and Applied Science, Santa Fe, 1985,* edited by P. G. Young *et al.* (Gordon and

Breach, New York, 1986), p. 1079.
[31]J. Rapaport, V. Kulkarni, and R. W. Finlay, Nucl. Phys. **A330**, 15 (1979).
[32]J. Rapaport, Phys. Rep. **87**, 25 (1982).
[33]R. D. Lawson, P. T. Guenther, and A. B. Smith, Phys. Rev. C **36**, 1298 (1987).
[34]R. D. Lawson, P. T. Guenther, and A. B. Smith, Phys. Rev. C **34**, 1599 (1986).
[35]P. A. Moldauer, Nucl. Phys. **47**, 65 (1963).
[36]F. G. Perey, computer code GENOA, private communication (1975).
[37]R. W. Finlay, *International Conference on Neutron Physics, Kiev, 1987* (Academia Nauka, Moscow, 1987).
[38]C. E. Brown and M. Rho, Nucl. Phys. **A372**, 397 (1981).
[39]J. P. Jeukenne and C. Mahaux, Nucl. Phys. **A394**, 445 (1983).
[40]T. R. Mo and R. H. Davis, Phys. Rev. C **6**, 231 (1972).